Computational Materials Science 184 (2020) 109935

Contents lists available at ScienceDirect

Computational Materials Science

journal homepage: www.elsevier.com/locate/commatsci

Influence of rolling temperature on the structural evolution and residual stress generation of nanocrystalline Nickel during nano-rolling process

K. Vijay Reddy, Snehanshu Pal*

Department of Metallurgical and Materials Engineering, National Institute of Technology Rourkela, 769008, India

ARTICLE INFO

Keywords:
Nano rolling
Nanocrystalline nickel
Residual stress
Virtual diffraction

ABSTRACT

Although the rolling process is significant on developing the preferred crystallographic orientation in the metallic sheets, its implementation at the nanoscale is uncertain. However, it is believed that the nano-rolling process can be realized with progressive scientific and technological advancement in material processing. Presently, we have modeled the rolling process of nanocrystalline Ni specimen using molecular dynamics simulations and investigated the underlying deformation mechanism along with the orientation evolution. Moreover, we have also analyzed the effect of temperature on the residual stress generation and the grain rotations. This atomistic model takes both shear and compressive forces into consideration, which makes it efficient in representing the actual deformation process. It is found that the compressive stress accumulation majorly occurs at grain boundary whereas tensile stresses are accumulated at triple junctions. At elevated temperatures, the stresses during the deformation are diminished and gets dispersed due to the thermal vibrations caused by the high temperature deformation. Through this study, we have evidently shown the orientation change, grain refinement, and formation of sub-grain boundaries during the rolling process. In addition, we have also characterized the specimens with virtual diffraction analysis, which has shown the preferred orientations to be (0 0 2) and (1 1 1) after rolling through the first and second set of rollers respectively.

1. Introduction

Nanocrystalline Nickel (NC Ni) system is known to possess excellent mechanical and thermo-physical properties [1–6], which makes it a good candidate for advanced functional and structural applications [7–9]. With such favorable properties, this metallic system can be utilized in numerous applications such as components for steam generators, turbines, heat exchangers [10,11], and in electromechanical devices [12]. For instance, Do and Lund have reported the efficacy of NC Ni system for undercoating barriers in electrical connectors with improved corrosion and wear resistance properties [13]. Apart from the bulk applications, these nanoscale metallic systems have a wide utility at due to their unique properties, which makes them a potential candidate for components in advanced functional applications [14]. Still, to explicitly use NC Ni in many of these components, the material has to be manufactured in the form of sheets and foils. Towards this perspective, the thin films are most produced by techniques such as electrodeposition [15,16], sputtering [17], and severe plastic deformations (SPD) [18,19]. However, the grains that are formed using these techniques are usually found to be having random crystallographic orientations [20–22]. It is known that some preferred grain orientations can substantially influence the structural and mechanical properties of the nano-scale metallic systems and subsequently define the product efficiency [23–25]. For this reason, it is necessary to develop a nano-processing technique that can induce textured grains in the nano-scale metallic system. But the present technology is inefficient in economically designing, processing, characterizing, and large-scale manufacturing of the textured sheets/foils at the nanoscale level. In general, the equipment set-up for the deformation of metallic system at nanoscale can be difficult and costly. Moreover, repetitive experimental analysis to optimize the process parameters can be sluggish, which results in the increase of the production cost and thus is not economical. Though, there are few nano-processing techniques available such as nano-machining [26–28] and nano-forming [29,30] to tailor and design application specific nano-scale engineering components; there exists no such method for producing textured nanocrystalline metallic sheets and foils.

Rolling process has a significant impact on developing the preferred crystallographic orientation in the finished metallic sheets. Extensive research efforts have already been put to understand the influence of rolling process on the structural manipulation and its effect on the material properties [25,31–34]. For instance, Ye et al. have studied the

* Corresponding author.
E-mail address: snehanshu.pal@gmail.com (S. Pal).

https://doi.org/10.1016/j.commatsci.2020.109935
Received 1 April 2020; Received in revised form 3 July 2020; Accepted 11 July 2020
Available online 23 July 2020
0927-0256/

surface properties of pure titanium and found that ultrasonic surface rolling produces lower coefficient of friction [31]. Similarly, Jinlong and Hongyun have analyzed the corrosion properties of pure iron and revealed that finer grain size aids in enhancing the corrosion resistance property of the material [32]. On the other hand, Suwas and Gurao have reviewed the impact of rolling process on the development of texture and its influence on mechanical properties such as strength and toughness, elastic properties, electrical properties, and wave/acoustic properties [25]. Even though the rolling process is a well-established method to deform the bulk nanostructured metallic systems, its realization at the nanoscale is still uncertain. Nano-rolling has been recently coined processing technique that deals with rolling of the nano-scaled metallic systems and transforming them into sheets and then understanding the core deformation mechanisms and texture evolution [35–39]. Although the experimental setup of this process has not been established yet, but with the progressive scientific and technological advancement in material processing, it is believed that this futuristic processing technique: nano-rolling process can be an extended part of traditional rolling process. In this viewpoint, researchers have already developed nano-roll forming techniques at nanoscale which are quite similar to that of the nano-rolling process [40,41]. Currently, the deformation mechanism, structural evolution, and texture analysis of the nano-rolled specimens are investigated using molecular dynamics (MD) simulation [35–39]. Specifically, MD is an efficient tool for studying and understanding the underlying physics behind the nano-level deformation mechanisms, grain orientation, defect evolution, and phase transformation under static, dynamic, and impact loading conditions [42–44]. Moreover, with the usage of discrete and small time-steps, frame-by-frame analysis of the deformation process can be studies which can be difficult and expensive using experimental techniques [45]. With respect to the nano-rolling process, we have developed an atomistic model taking into consideration both the shear and the compressive forces that act on the nanocrystalline material during the deformation process, which make it capable in mimicking the actual deformation mechanisms. In the present investigation, we have implemented MD simulations to study the influence of rolling temperature on the deformation behavior of NC Ni during the nano-rolling process. Moreover, we have also investigated the effect of the reduction percent on the residual stress generation and the texture evolution of the specimens. We have also performed various analyses such as polyhedral template matching (PTM) [46], orientation scatter analysis [47], dislocation analysis [48], atomic stress analysis [49], and virtual diffraction analysis [50,51]. The simulation setup of the roller and the specimen and the results obtained through analyses has been presented in the subsequent sections.

2. Computational methods

2.1. Preparation of nanocrystalline Ni specimen

A model of single crystal (SC) Ni having dimensions of (30 × 15 × 20) nm is first separately created and then relaxed by performing the energy minimization using the conjugate gradient method [52] with a force and energy tolerance of 10^{-6} eV/Angstroms and 10^{-8} respectively (step 1 of Fig. 1(a)). The SC preparation and the energy minimization process is carried out using open source LAMMPS package [52] and the atomic interactions are described through Embedded Atom Method (EAM) interatomic potential developed by Mendelev et al. [53]. In order to create a nanocrystalline specimen out of the SC Ni, Voronoi tessellation method is employed using the Atomsk platform [54]. This method separates the simulation box into domains to create the representative volume element (RVE) into polygons depending on the distances between the nodes [55]. Hence, in order to generate the domains, few interconnected nodal points inside the simulation box of SC Ni having distinct spatial positions and random distribution are introduced (step 2 of Fig. 1(a)). These nodes are also known as seeds or nucleating nodes and are specified with a set:

$$\boldsymbol{g} = \{g_1, g_2, \cdots\cdots g_m\},\ g_i \in \mathbb{R}^n \tag{1}$$

This indicates that each and every atom in the space, $x \in \mathbb{R}^n$ is associated with the nearest nucleating node. This phenomenon is schematically demonstrated in the step-2 and step-3 of Fig. 1(a), which shows the defined contours that, constitutes the future grains to be formed. Here, the centers of the RVE are placed at ordered bcc superlattice sites in the simulation box, which resulted into the generation of the grains in the form of truncated octahedron shape (when viewed in 2-dimesion, gives the shape of a regular hexagon). After the RVE selection, the orientation of the seed is altered through rotation, such that the entire orientation of the space, $x \in \mathbb{R}^n$ is modified. In this process, the overlapping atoms in the specimen are deleted by providing a cut-off value. During the grain rotation, few of the atoms also lie outside of the simulation box, thus creating voids. To remove such voids, we have implemented the wrap function from the Atomsk software [54]. The purpose of the wrap command is to translate the atoms that are outside of the simulation box by few lattice vectors such that all the atoms end up in the simulation box. By this way, the voids are filled up and a periodic specimen is generated. Finally, the misorientations of the domains lead to the formation of the grain boundaries resulting into a polycrystalline specimen as shown in the final step of Fig. 1(a). During the entire NC specimen preparation process, periodic boundary conditions have been implemented in all the three directions. We have once again performed energy minimization of the NC specimen using conjugate gradient method [52] followed by equilibration at the specific rolling temperatures (i.e. 77 K, 300 K, and 900 K) under NPT ensemble. This process aids in the relaxation of the grain boundaries and the triple junctions in the specimen before the initiation of the rolling process. A three-dimensional (3D) atomic snapshot of the specimen along with the final dimension (30 × 20 × 15) nm is illustrated in Fig. 1(b). As the NC specimen is obtained from the rotation of set of atoms, we have quantitatively presented the distribution plot of the atomic percentage that has been rotated to obtain the polycrystalline structure in Fig. 1(c). The grain rotation analysis is carried out through post-processing of the specimen in the open source visualization software OVITO [56]. The NC Ni specimen consists of 16 grains in total and the grain size distribution is presented in Fig. 1(d). In order to determine the grain diameter, we have simplified the calculation by assuming the shape of the truncated octahedron grain as a sphere. After that, the volume of the grains is determined and the average diameter of the grain is calculated, which is found to be approximately 9 nm. It is observed that only a few percent of atoms/grains are low angle rotations (less than 15° rotation) whereas most of the grains have been rotated greater than or equal to 30°. We have analyzed through Centro-symmetry parameter (CSP) and dislocation analysis that the NC Ni specimen generated from the Voronoi tessellation method has high angle grain boundaries separating the grains. Fig. 2(a) illustrates shows the CSP snapshot of the specimen and it is observed the absence of periodic arrangement (or repeating units) of the GB structure. This indicates that the GBs is high angle boundaries and cannot be described through the coincidence site lattice (CSL) theory. On the other hand, the dislocation snapshot shows the absence of array of misfit dislocations at the interface of any two grains indicating that the misalignment between the grains are large and the interface is high angle grain boundary (refer Fig. 2(b)).

2.2. Model setup of the specimen-roller assembly

The NC specimen prepared is then merged with the rollers to create the specimen-roller setup for the rolling process. The atomic snapshot of the NC Ni specimen having the dimension of (30 × 15 × 20) nm along with the two set of rollers is shown in Fig. 3(a). The two set of rigid all-atom cylindrical rollers are constructed having a face-centered cubic (fcc) crystal structure. The diameter of the rollers is 14 nm with a total

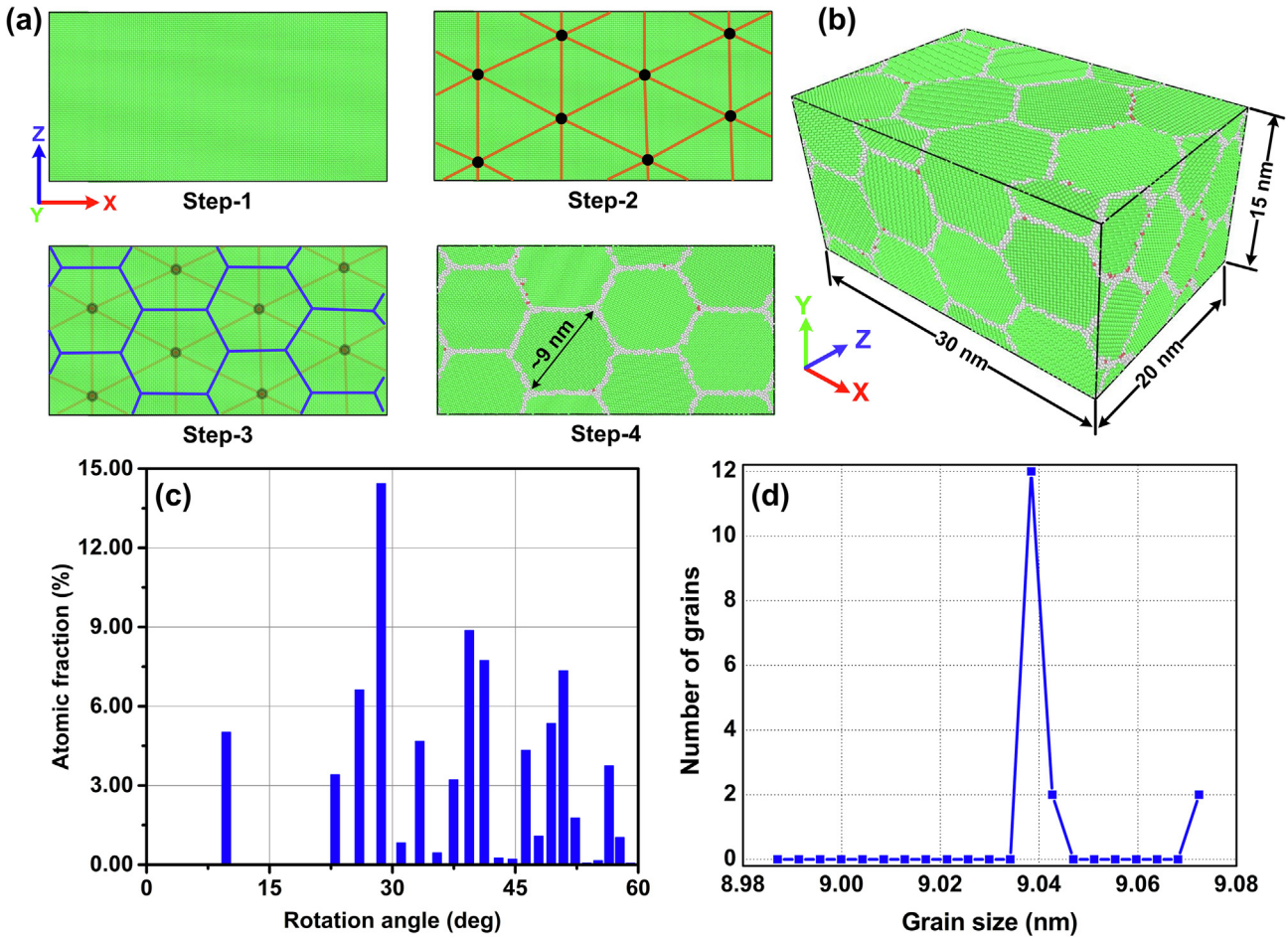

Fig. 1. (a) Illustration of step-by-step process of preparing nanocrystalline Ni specimen using Voronoi tessellation method, (b) Atomic snapshot of the NC Ni specimen along with the dimensions, (c) Rotation angle vs. atomic fraction plot showing the distribution of atomic rotation during the preparation of NC specimen through single crystal Ni, (d) Grain size distribution of the NC Ni specimen.

length of 20 nm and are positioned in such a way that the separation distance between them is ~13.8 nm (8% thickness reduction) and ~10.8 nm (20% thickness reduction). Here, we have considered all-atom rollers instead of rigid rollers (without atoms) to consider the effect of shear stress that is induced due to the roller-specimen atomic interactions during the roller rotation. On the other hand, the rigid rollers (without atoms) can only impart compressive forces on the specimen as there is no effect of rotation on the specimen. The rollers are rotated such that the upper roller in both the sets moves in an anti-clockwise direction whereas the lower rollers move in a clockwise direction. The total number of atoms in the entire set-up (specimen and the rollers) is ~2 million atoms. We have specified the rolling direction

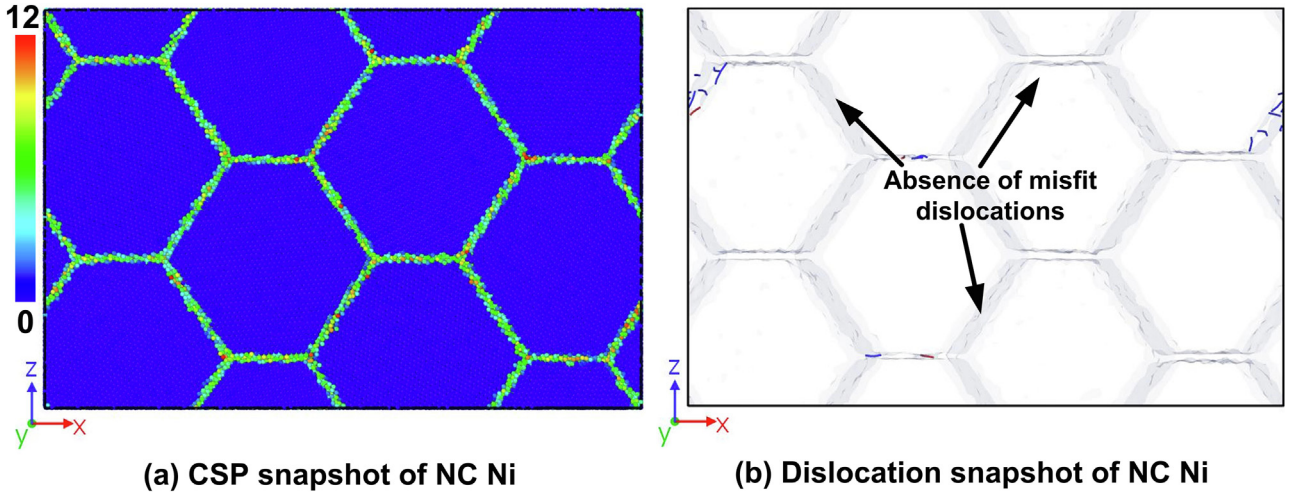

Fig. 2. (a) Illustration of the centro-symmetry parameter (CSP) snapshot of the initial NC Ni specimen, (b) shows the absence of misfit dislocations at the grain boundary of the initial specimen.

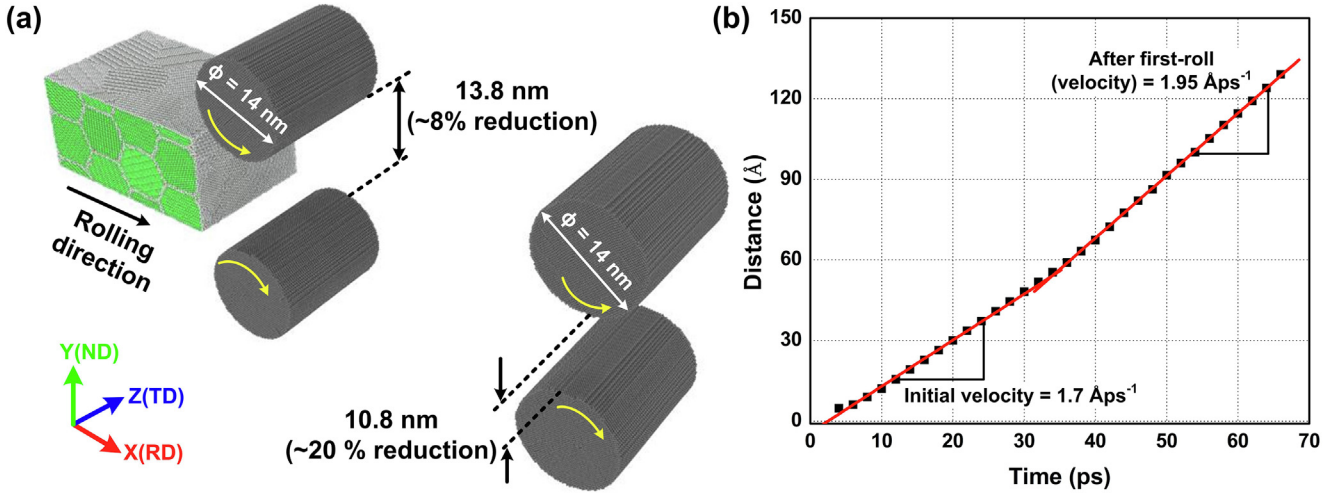

Fig. 3. (a) Atomic snapshot of the NC Ni specimen along with the two set of rollers for the nano-rolling process. The reduction thickness (and percentage) during the passing of each roller is specified. Here, RD indicates rolling direction, TD indicates transverse direction, and ND indicates normal direction, (b) Plot illustrating the distance vs. time plot during the rolling of NC Ni specimen through the first set of rollers. The red lines indicate the slope (velocity) before and after the rolling process.

(RD) along X-axis, normal direction (TD) along Y-axis, and transverse direction (ND) along Z-axis. The nano-rolling process of the specimen is carried out at three different temperatures, i.e. 77 K, 300 K, and 900 K to investigate the temperature effect on the overall stress generation, plastic deformation, and grain orientation of the rolled NC specimens. These three particular temperatures have been chosen in order to comprehend the deformation behavior at cryogenic condition (77 K), room temperature condition (300 K), and a high temperature condition (900 K) for the Ni system. Also, it is to be noted that the same initial NC Ni specimen is used for all three rolling temperature conditions. After the model setup, the system is equilibrated at these temperatures under NVE ensemble (micro-canonical ensemble, where N is the total number of atoms, V is the volume, and E is the energy) and Nosé-Hoover thermostat [57]. A 2 fs time step is used for carrying out the entire nano-rolling simulation. The boundary conditions of the setup are changed to non-periodic and shrink wrapped along the RD and ND, whereas periodic boundary conditions are used in the TD. After initiation of the rolling process, we have implemented NVT ensemble (canonical ensemble, where N is the number of particles, V is the volume, and T is the temperature). During the nano-rolling deformation, the specimen is driven forward along the RD by providing a constant velocity to the specimen. Upon traversing through the rollers, the thickness of the specimen reduces and consequently the velocity increases. The relation between the specimen velocity and thickness is mathematically represented as:

$$h_0 V_0 w_0 = h_1 V_1 w_1 \tag{2}$$

where, h_0, h_1 is the initial and final thickness, V_0, V_1 the initial and final velocity, w_0, w_1 the initial and final width respectively. Since, the width is maintained constant through periodic boundary conditions, Eq. (2) changes to:

$$\frac{h_0}{h_1} = \frac{V_1}{V_0} \tag{3}$$

From the Eq. (3), we can relate the velocity change with respect to the thickness reduction of the specimen. As a representative case, we have considered the change in the velocity of the specimen during the traversing through the first set of rollers. Fig. 3(b) shows the distance vs. time plot during the rolling process and the slope indicates the velocity of the specimen. The initial specimen velocity is found to be 1.7 $Åps^{-1}$ and the final velocity after traversing out of the first set of rollers is 1.95 $Åps^{-1}$ for a thickness reduction of 8 percent. On comparing the calculated value from Eq. (3) (1.84 $Åps^{-1}$) with the obtained value from the MD simulation, we have observed only a small deviation in the final velocity of the specimen.

2.3. Determination of lattice orientation and stress

In order to identify the lattice orientations and the subsequent grain rotation during the nano-rolling, we have implemented an algorithm to determine the local lattice using Polyhedral Template Matching (PTM) [46]. The reason behind using Polyhedral Template Matching method over Common Neighbor Analysis (CNA) [58] is that the former method is better suited in determining the structural evolution during high strain (plastic) deformations [46]. The analysis of the determination of the orientation of the rolled specimens is carried out by post-processing the simulation data using open source visualization software OVITO [56].

The calculated orientations are stored as quaternion values and the lattice orientations are visualized (in the form of RGB colors) by using a python modifier. In general, a quaternion that is signified by $\boldsymbol{q}$ is a set of scalar and vector elements $[q_0, q_1, q_2, q_3]$ and mathematically represented as [48]:

$$\boldsymbol{q} = q_0 + iq_1 + jq_2 + kq_3 \tag{4}$$

where, q_0 is the scalar term and q_1, q_2, q_3 are the vector terms. Hence, the mathematical representation of equation (4) can also be given as:

$$q = \langle s,\ V \rangle \tag{5}$$

In case of nano-rolling process, the deformation causes the rotation of the grains for which the quaternion values $[q_0, q_1, q_2, q_3]$ can be linked with the change in the rotation axis and the angle of rotation through a unit vector, $\boldsymbol{\xi}$ using the following mathematical expression [47]:

$$\boldsymbol{q} = \cos\left(\frac{\omega}{2}\right) + \boldsymbol{\xi}_1 \sin\left(\frac{\omega}{2}\right) + \boldsymbol{\xi}_2 \sin\left(\frac{\omega}{2}\right) + \boldsymbol{\xi}_3 \sin\left(\frac{\omega}{2}\right) \tag{6}$$

$$\text{or, } \mathrm{q} = \left\langle \cos\left(\frac{\omega}{2}\right), \xi_i \sin\left(\frac{\omega}{2}\right) \right\rangle \tag{7}$$

where, the angle of rotation (ω) is represented by the scalar term: $\cos\left(\frac{\omega}{2}\right)$ and the rotational axis is determined by the vector term: $\xi_i \sin\left(\frac{\omega}{2}\right)$. Fig. 4 schematically shows that the axis rotation of the grains in the specimen can be quantified through the values q_1, q_2, q_3 whereas the angle of rotation can be quantified through the value ofq_0. Here, we

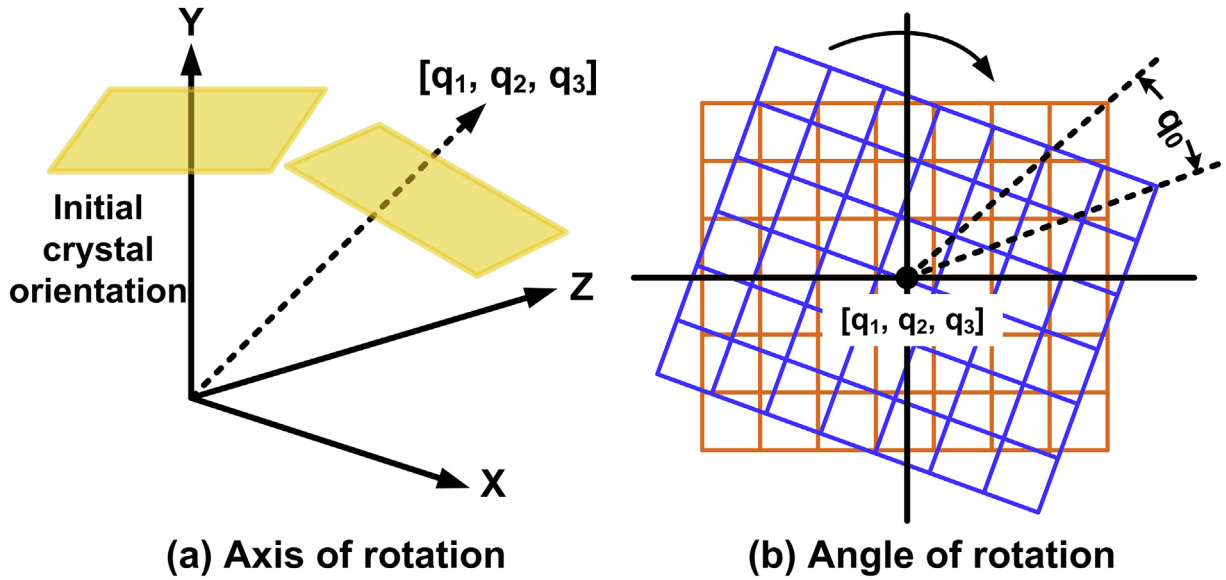

Fig. 4. Schematic illustration of (a) axis of rotation, and (b) angle of rotation represented through the four set of quaternion values during the nano-rolling process.

have initially considered the NC Ni specimen with an initial grain size of 9 nm; however, new grains with different lattice orientations are formed after the nano-rolling process. We have calculated the angle of rotation (ω) by using the first term of the computed quaternion and then, the obtained value of ω is used to find the rotational axis (ξ_i) using the three vector quaternion terms.

3. Results and discussion

3.1. Structural evolution and stress distribution during cryo-rolling

Fig. 5 illustrates the atomic stress snapshots and the stress distribution plot during the rolling of specimen through the first set of rollers (8% thickness reduction) at 77 K temperature. Before the initiation of the nano-rolling process, it is observed that the specimen has approximately zero stress in the bulk region whereas small quantity of compressive and tensile stress is present at the grain boundaries (GBs). Fig. 5(a-d) shows the generation of compressive stress (σ_{yy}) along the normal of the specimen rolling direction, which aids in the reduction of the thickness of the specimen. From the atomic snapshots, it is clearly observed that a localized residual compressive stress is accumulated at the grain boundary (GB) region after the specimen traverses out of the first set of rollers. Moreover, a tensile residual stress is also found to be accumulated at the triple junction of the GB indicating high stresses at the interfacial regions (refer Fig. 5(d)). Accretion of such stresses in the specimen can likely helps in grain refinement and increasing the mechanical behavior of the material [59,60]. Fig. 5(e) shows the stress distribution plot for the specimen before entering the rollers, during the process, and the rolled NC specimen. The peak of the stress distribution is lowest during the process, which indicates that a comparatively higher intensity of compressive stress is generated. The finding from the plot is in good agreement with that of the atomic snapshots shown in Fig. 5(a-d). Upon traversing out of the rollers, the peak of the stress distribution in the specimen shows a similar value to that of during the rolling process indicating that the specimen has been plastically deformed. Though, after the specimen is out of the rollers, the excessive compressive stress is relieved and quantitatively the stress value decreases. However, the inset of Fig. 5(e) shows the grey shaded region, which indicates the presence of final compressive residual stress in the specimen. After passing through the first set of rollers, the specimen

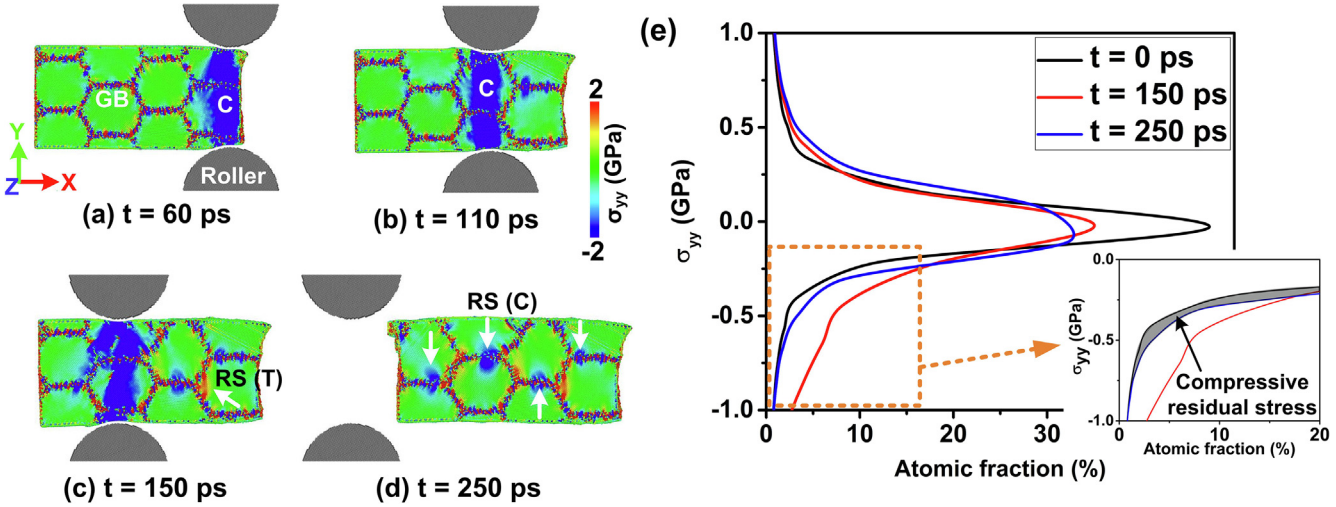

Fig. 5. (a-d) Atomic snapshots illustrating the normal stress distribution (σ_{yy}) in the specimen during the rolling deformation process through the first set of rollers at 77 K, (e) Atomic fraction vs. stress plot showing the quantitatively the distribution of stress at initial, during and after the rolling process for the first set of rollers. Inset indicates the residual stress after the rolling process.

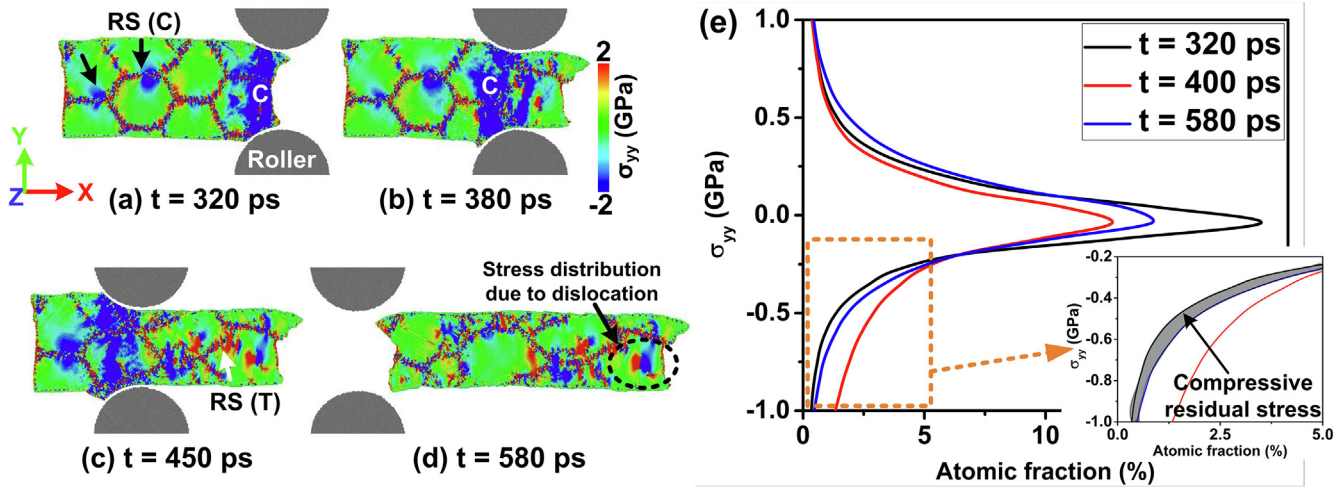

Fig. 6. (a-d) Atomic snapshots illustrating the normal stress distribution (σ_{yy}) in the specimen during the rolling deformation process through the second set of rollers at 77 K, (e) Atomic fraction vs. stress plot showing the quantitatively the distribution of stress at initial, during and after the rolling process. Inset indicates the residual stress after the rolling process.

then moves towards the second set of rollers with a comparatively higher reduction percent (~20% reduction). Fig. 6 shows the qualitative distribution of the stress through atomic snapshots and the quantitative stress distribution plot during the nano-rolling through the second set of rollers. Similar to the previous case, a localized compressive stress (σ_{yy}) is generated near the region of roller-specimen contact as shown in Fig. 6(a-d). However, after the specimen has passed through the rollers, both tensile and compressive residual stresses are observed in the specimen. This is attributed to the higher degree of deformation that has caused the generation of larger number of dislocations to accommodate the plastic strain. We have specifically shown the tensile-compressive stress field that has been formed due to the edge dislocation in Fig. 6(d). The dislocation generation and the structural evolution due to the comparatively higher reduction rate have been discussed later in this paper. Fig. 6(e) illustrates the quantitative distribution of the normal stress acting on the NC Ni specimen during the rolling process through second set of rollers. It is observed that the amplitude (near zero stress) first decreases during the deformation with a generation of larger compressive stress and then slightly increases after the specimen is out of the rollers. Compared to the previous rolling conditions (lower compression percent), the increase in the atomic fraction amplitude (at the zero stress) after rolling can be attributed to the dislocation annihilation and formation of dislocation substructures.

Fig. 7(a) exemplifies the initial grain rotation plot along with the orientation snapshot and schematic of relation between rotation angle and quaternion q_0. The grains are colored with different combination of RGB colors depending upon their rotations with respect to the initial SC Ni specimen. After the deformation through the first set of rollers during cryo-rolling process (77 K), it is observed that the change in the atomic fraction with respect to the rotation angle is minimal (refer the plot in Fig. 7(b)). This indicates that most of the grain orientations are constant, though small rotations are detected at few regions on the specimen surface (shaded region in Fig. 7(b)). The atomic stress distribution snapshot shows that high localized stresses are generated causing the change in the orientation at those regions. On further reduction in the thickness through rolling deformation, it is observed that the atomic fraction with low angle rotations decreases and consequently high angle rotations increases in the specimen (refer Fig. 7(c)). Also, the atomic stress distribution(σ_{xx}) shows that the region of high angle rotation is facilitated by the generation of large positive stress. The positive stress along the rolling direction denotes shearing of the specimen surface and indicates that the grain rotation is attributed to the shear stress during rolling, which is in good agreement with the literature studies [61,62]. In addition to the grain rotations, new orientations are also formed in the specimen through generation of smaller/finer grains separated through subgrain boundaries (refer orientation snapshot in Fig. 7(c)). In general, such deformation and grain rotations assist in the accumulation of the plasticity in the nano-rolled specimen at low temperatures. Similar mechanism of plastic deformation through the grain rotation has already been observed in nanocrystalline systems and is reported in the literature [63]. In order to elaborately analyze the structural evolution and orientation generation in the specimen after the cryo-rolling process, we have illustrated the final specimen surface orientation along with its corresponding dislocation structure as a representative case in Fig. 8. Subgrain boundaries and misfit dislocation (mostly Shockley partial dislocations) are observed to be formed between slightly different oriented grains. Moreover, two-dimensional meshes of dislocation structures are formed indicating the formation of low angle grain boundaries (LAGBs) along with the high angle grain boundaries (HAGBs). Few sessile dislocations such as stair-rod and Frank partials are also observed to be formed at few interfaces.

3.2. Stress analysis and orientation evolution during room temperature rolling

In this section, we have studied the deformation behavior, stress distribution and the texturing of the NC Ni specimen during the rolling process at 300 K temperature. Fig. 9(a-d) shows the atomic snapshots of the normal stress distribution in the specimen during the deformation through the first set of rollers. Similar to the cryo-rolling, the region of roller-specimen interaction generates a high compressive stress (negative stress) that aids in the reduction of the specimen thickness. However, it is observed that few localized regions having tensile stress (positive stress) are present near the grain boundary junctions upon traversing out of the rollers as shown in Fig. 9(d). Quantitative analysis through atomic fraction vs. stress plot also shows that the final specimen (after rolling through the first set of rollers) has a positive residual stress due to the stress accumulation at triple junctions. The finding from the stress analysis is in good agreement with that of the experimental studies of cold-rolling process [64,65]. After the initial rolling, the specimen is passed through the second set of rollers, which has a thickness reduction percent of 20% (higher strain). Fig. 10 demonstrates the atomic stress snapshots along with its quantitative distribution during the deformation process. It is observed that the stress generation during the rolling is similar to that of the previous case

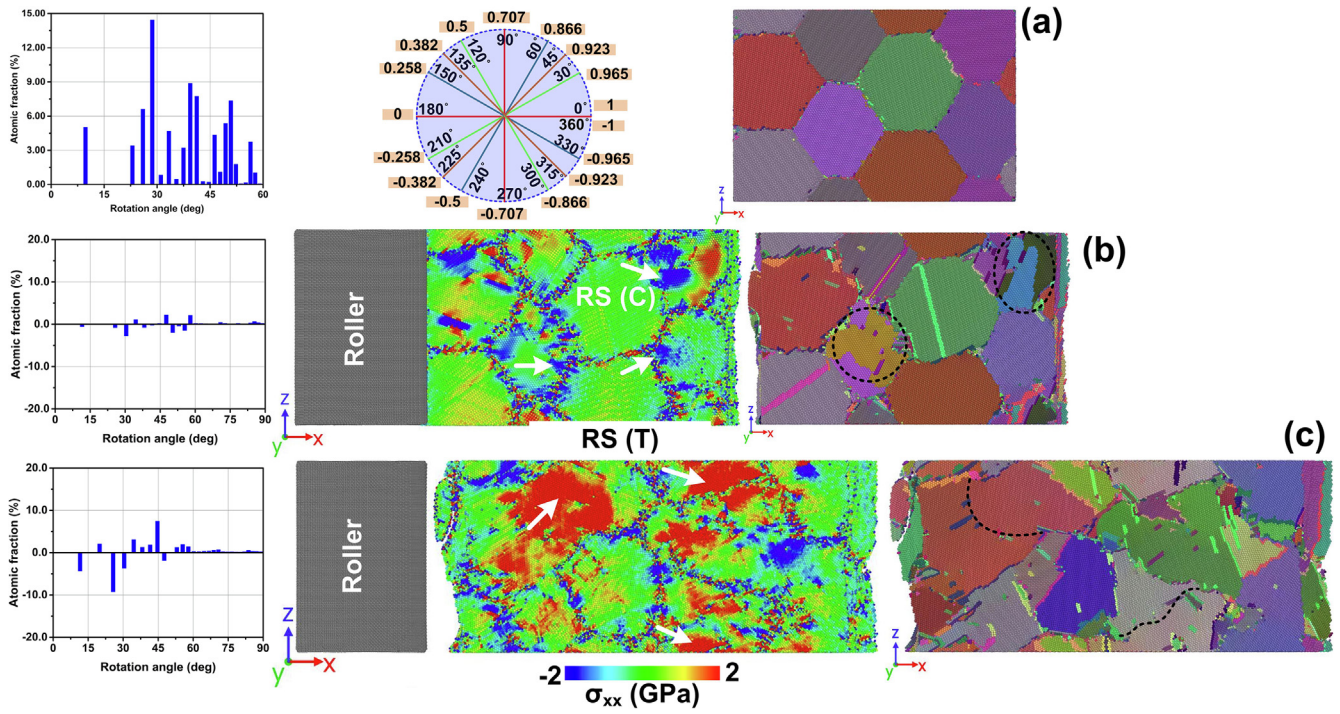

Fig. 7. (a) Initial grain rotation distribution along with the schematic of relation between rotation angle and quaternionq_0 and the orientation of the initial NC Ni specimen, (b) atomic rotation plot along with the stress distribution(σ_{xx}) and the orientation of the NC Ni specimen during the first set of rollers at 77 K, (c) atomic rotation plot along with the stress distribution(σ_{xx}) and the orientation of the NC Ni specimen during the second set of rollers at 77 K.

(refer Fig. 6); however, a larger region in the specimen show the compressive-tensile stress field that is a characteristic feature for the presence of dislocations (perfect or partial dislocations, refer Fig. 10(d)). Moreover, the deformation has also caused the distortion of the grain boundaries in the specimen resulting in the change of the grain shape. Quantitative analysis also shows the presence of a small tensile residual stress in the specimen whereas the compressive stress has been reduced, which indicates that the elevated temperature (300 K) has aided in the stress relaxation (refer Fig. 10(e)). Such stress relaxation phenomenon is generally not observed during the cold rolling process and needs additional annealing of the specimen but here, due to the nanoscale structure and close proximity between the surfaces, defect annihilation is prominent leading to relaxation.

In order to analyze the grain orientation scatter in the NC Ni specimen during the deformation through the first and second set of rollers, we have plotted the rotation angle vs. atomic fraction graphs along with the stress and orientation snapshots obtained through the quaternion analysis (refer Fig. 11). The orientations are denoted through the various combinations of RGB colors depending on the grain rotations with respect to the initial configuration. It is observed that the change in the grain rotations after the first rolling condition is minimal as the thickness reduction percent is lower. Nevertheless, it is found that few localized regions at the surface of the specimen show generation of new orientations along with the creation of finer grains. Studies have shown that the surface atoms have lesser constraints than the interior atoms and hence the rotation is more favorable [66]. Moreover, there is generation of few twin boundaries in the specimen to accommodate the plastic strain (refer Fig. 11(b)). Upon increasing the thickness reduction percent, an increase in the high angle atomic rotation is observed at the expense of reduction in the low angle rotations. On the other hand, the atomic stress snapshot shows large patches of positive stress indicating the shearing on the surface of the specimen (refer Fig. 11(c)). Overall, the previous results and the current stress snapshot indicate that the residual negative stress (compression) is released after the entire nano-rolling process at 300 K. The corresponding orientation snapshot reveals distortions of original hexagonal grains and formation of smaller grains with new orientations. Also, the grain near the high positive stress region has shown complete change in the

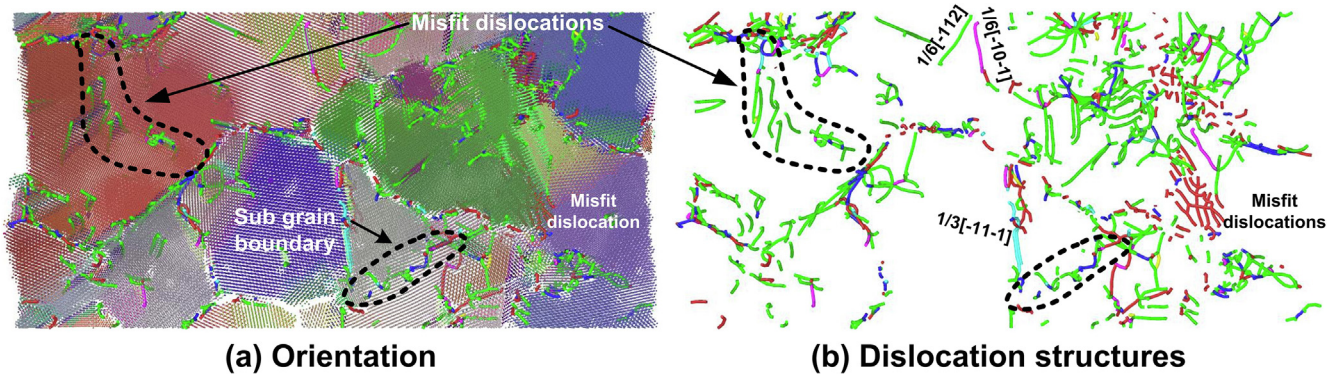

Fig. 8. Atomic snapshot illustrating the surface of the cryo-rolled specimen after the rolling through the second set of rollers along with the dislocation structures that are generated during the deformation process.

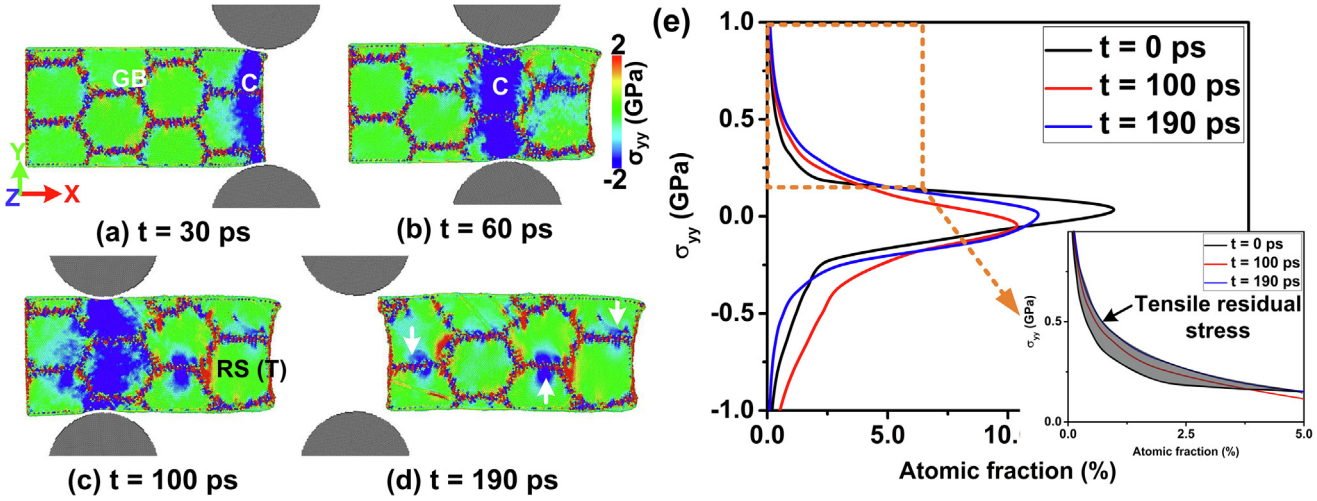

Fig. 9. (a-d) Atomic snapshots illustrating the normal stress distribution (σ_{yy}) in the specimen during the rolling deformation process through the first set of rollers at 300 K, (e) Atomic fraction vs. stress plot showing the quantitatively the distribution of stress at initial, during and after the rolling process. Inset indicates the residual stress after the rolling process.

RGB color signifying high angle grain rotation (refer Fig. 11(c)).

3.3. Stress analysis and texture evolution during hot rolling

Fig. 12(a-d) illustrates the atomic snapshots of the normal stress distribution (generated due to the rollers) in the specimen at different time intervals of nano-rolling process (through first set of rollers). Also, a quantitative stress distribution is presented through stress vs. atomic fraction plot to determine the development of residual stress after the rolling process (refer Fig. 12(e)). As observed in the previous cases, a compressive stress (σ_{yy}) is generated at the roller-specimen interaction region (refer Fig. 12(a-c)). Apart from this, the overall specimen shows small stresses in the grain interior that can be attributed to the thermal vibrations caused by the high temperature deformation. Also, due to the elevated temperature, the atomic stress is found to be dispersed in the specimen indicating a homogenous distribution of stress. This can be correlated with the low amplitude (zero stress) in the stress distribution plot at the initial stages of rolling (refer Fig. 12(e)) as compared with the previous cases of low temperature rolling. Once the specimen traverses into the rollers (at t = 60 ps), it is observed that the central region of the specimen does not experience much compressive stress due to the rollers. Hence, the decrease in the amplitude in the plot is also slightly less when compared to the low temperature deformation. After the specimen comes out of the rollers, the atomic snapshot shows formation of tensile-compressive stress fields indicating the formation of dislocations in the specimen. However, quantitatively, the overall residual stress due to the high temperature nano-rolling process is low as indicated in the inset of Fig. 12(e).

Fig. 13 shows the stress snapshots along with the distribution plot during the rolling process of the NC specimen through the second set of rollers at 900 K temperature. Due to the large reduction percent, a larger compressive stress is generated at the roller-specimen interaction, though a tensile residual stress is formed when the specimen moves out of the rollers. This leads to the decrease in the atomic fraction at zero stress region and uniform increase at both tensile and compressive stress region as shown in Fig. 13(e) at 150 ps. Upon completion of the deformation process, a tensile residual stress is observed in the specimen, which is contrary to the low temperature deformation process. This can be attributed to the large grain distortions (through orientation change) that have occurred to accommodate the plastic strain during deformation, (which will be discussed in Fig. 15). Similar to the previous case, it has been observed that the specimen undergoes stress relaxation during the traversing in between the two rollers. It is already discussed that the stress relaxation process occurs

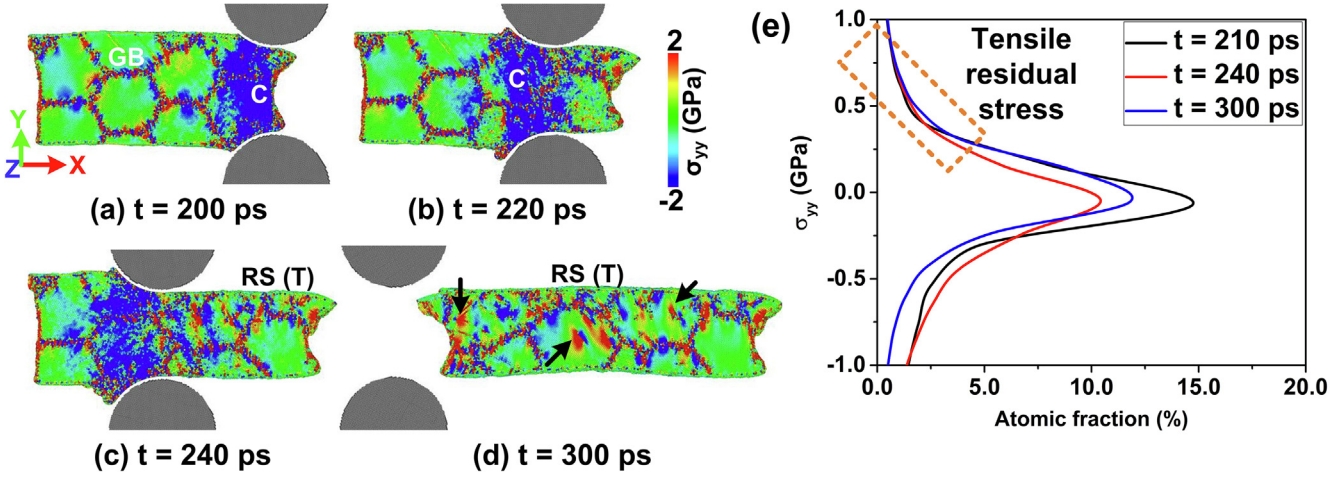

Fig. 10. (a-d) Atomic snapshots illustrating the normal stress distribution (σ_{yy}) in the specimen during the rolling deformation process through the second set of rollers at 300 K, (e) Atomic fraction vs. stress plot showing the quantitatively the distribution of stress at initial, during and after the rolling process. Inset indicates the tensile residual stress after the rolling process.

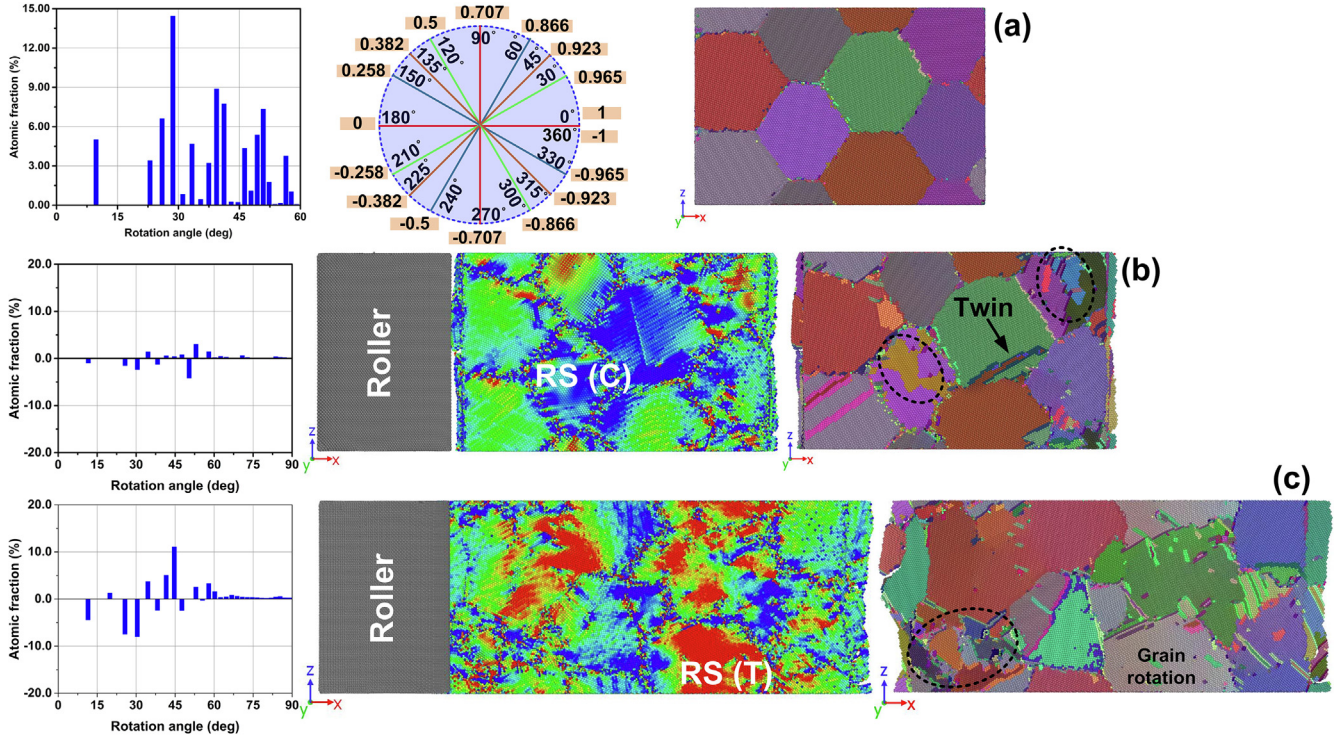

Fig. 11. (a) Initial grain rotation distribution along with the schematic of relation between rotation angle and quaternionq_0 and the orientation of the initial NC Ni specimen, (b) atomic rotation plot along with the stress distribution(σ_{xx}) and the orientation of the NC Ni specimen during the first set of rollers at 300 K, (c) atomic rotation plot along with the stress distribution(σ_{xx}) and the orientation of the NC Ni specimen during the second set of rollers at 300 K.

due to the nanoscale size of the specimen and close proximity between the surfaces, which causes defect annihilation (refer Fig. 10). Apart from the nano-scale size of the specimen, the traversing time between the two set of rollers is also important in the relaxation as it is a time-dependent decrease of stress in the specimen under constant strain. Fig. 14 quantitatively shows the stress relaxation of the NC Ni specimen before entering the second set of rollers during high temperature rolling process (900 K taken as a representative case). Fig. 14(a) illustrates the stress distribution of the atoms at different time period and it is observed that the fraction of atoms having zero stress value increases as the specimen moves towards the second set of rollers (~the total travel time in between the two set of rollers is 10 ps). Moreover, the maximum induced stress in the specimen also decreases with respect to time during the relaxation process (refer Fig. 14(b)). The increase at 110 ps indicate that the specimen has entered the second set of rollers (refer Fig. 13) due to which the maximum stress rises once again. The decrease of stress can be attributed to the fact that dislocation annihilation at elevated operating temperature is high. In this view, we have analyzed the variation of dislocation density and observed a continuous decrease with respect to traversing time (refer Fig. 14(c)). The trend of the plot indicates that the stress relaxation is due to the annihilation of the partial dislocations in the specimen. We have provided supplementary videos (Video V1 and V2) showing the nano-rolling process of NC Ni at 77 K and 900 K respectively.

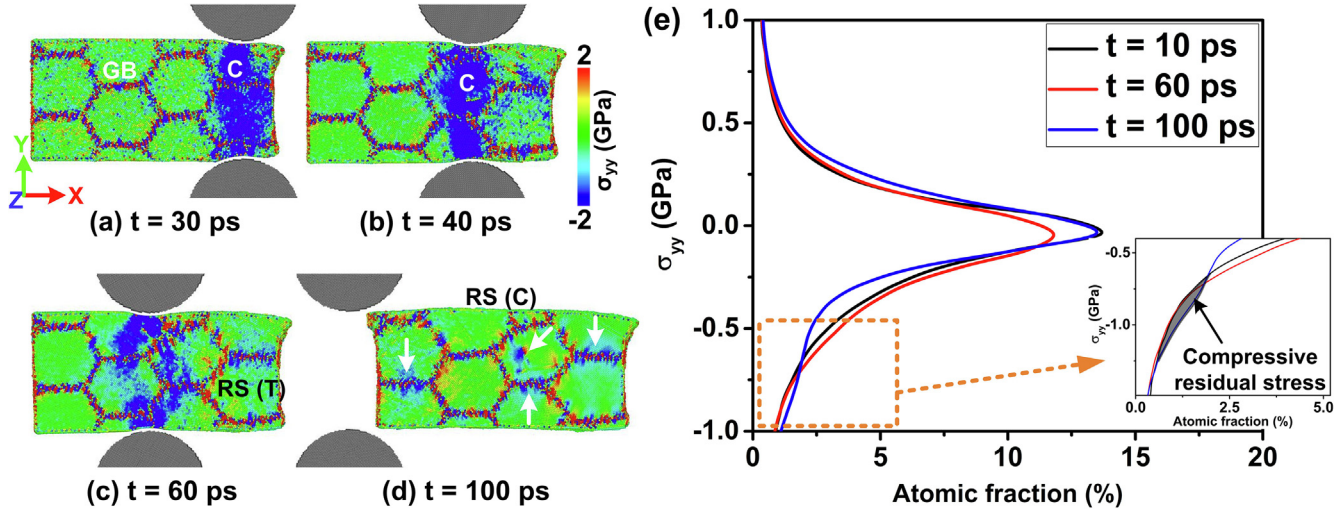

Fig. 12. (a-d) Atomic snapshots illustrating the normal stress distribution (σ_{yy}) in the specimen during the rolling deformation process through the first set of rollers at 900 K, (e) Atomic fraction vs. stress plot showing the quantitatively the distribution of stress at initial, during and after the rolling process. Inset indicates the compressive residual stress after the rolling process.

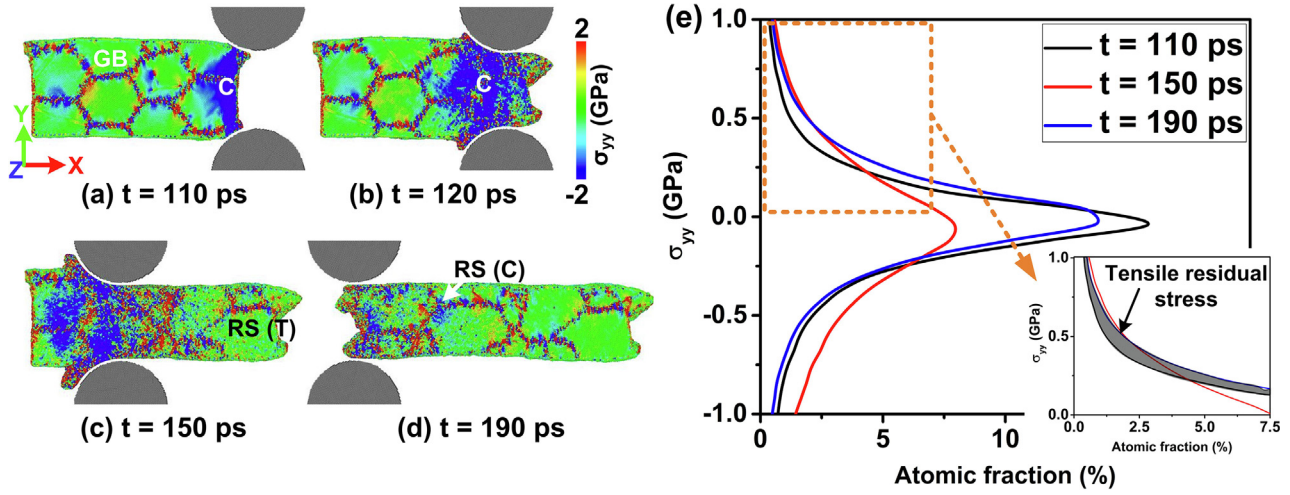

Fig. 13. (a-d) Atomic snapshots illustrating the normal stress distribution (σ_{yy}) in the specimen during the rolling deformation process through the second set of rollers at 300 K, (e) Atomic fraction vs. stress plot showing the quantitatively the distribution of stress at initial, during and after the rolling process. Inset indicates the tensile residual stress after the rolling process.

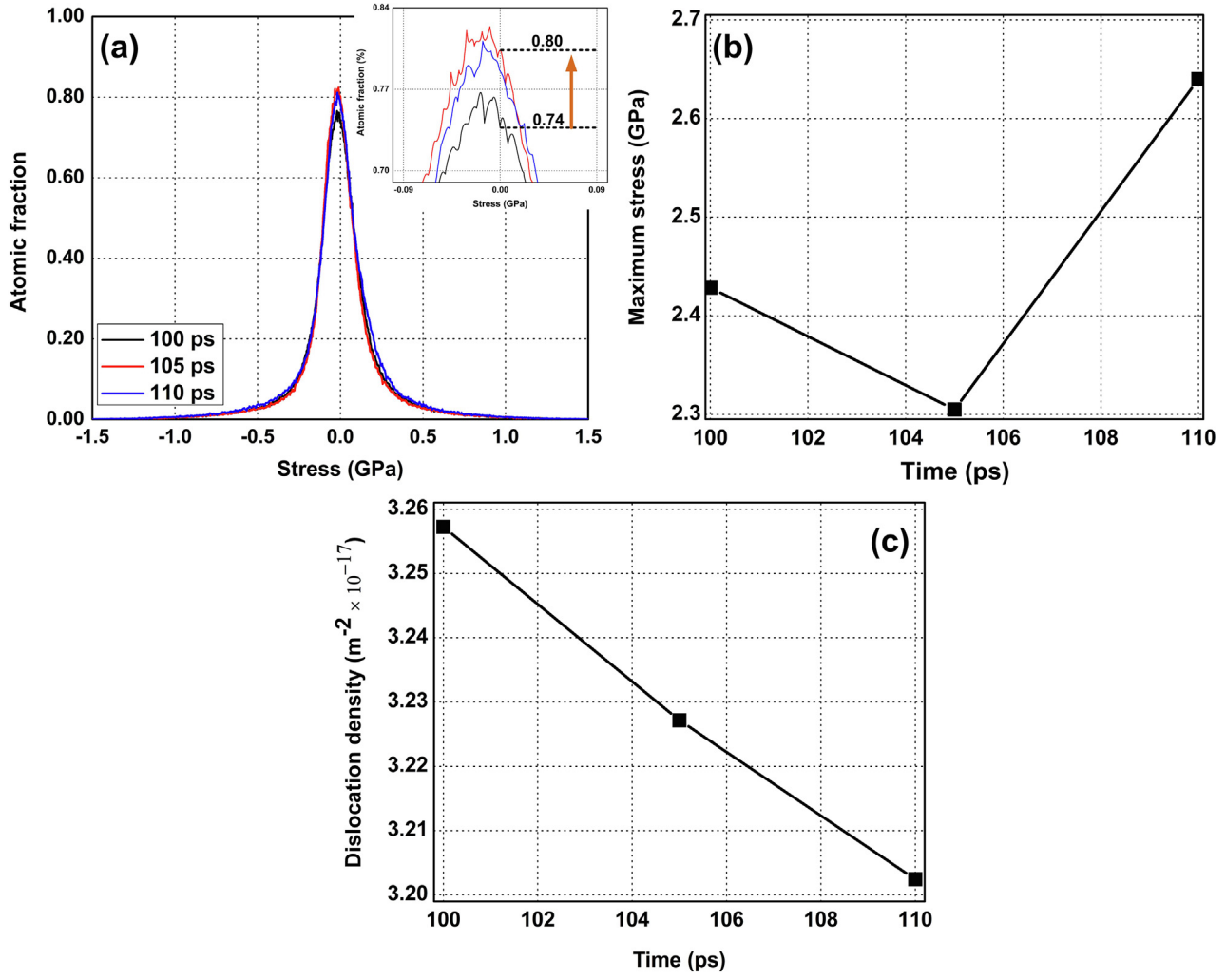

Fig. 14. (a) Plot shows the distribution of stress with respect to atomic fraction after rolling through the first set of rollers (100 ps), during the traversing towards the second set of rollers (105 ps), and the initial traversing of the specimen into the second set of rollers. Inset shows the variation in the atomic fraction at zero stress. (b) Plot shows the variation of maximum stress during the traversing of the specimen, whereas (c) shows the variation in the dislocation density for the same time period.

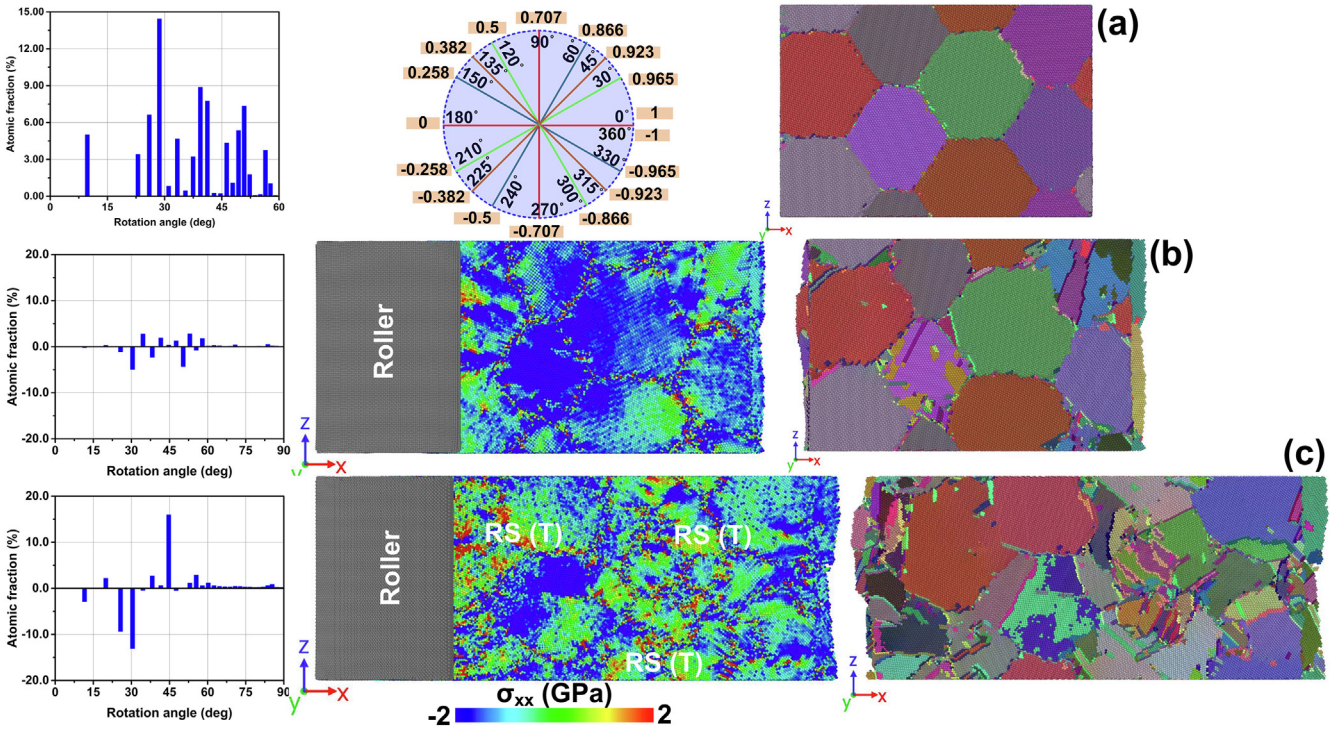

Fig. 15. (a) Initial grain rotation distribution along with the schematic of relation between rotation angle and quaternionq_0 and the orientation of the initial NC Ni specimen, (b) atomic rotation plot along with the stress distribution(σ_{xx}) and the orientation of the NC Ni specimen during the first set of rollers at 900 K, (c) atomic rotation plot along with the stress distribution(σ_{xx}) and the orientation of the NC Ni specimen during the second set of rollers at 900 K.

The atomic snapshots for the stress distribution and texture evolution during rolling through both set of rollers at 900 K temperature is depicted in Fig. 15. Also, rotation angle vs. atomic fraction plots are illustrated to determine the orientation change of the Ni atoms during the rolling process. It is observed that the magnitude of change in the rotation angles for the first set of rollers is comparatively higher than the lower temperature deformation. This indicates that the requirement of the stress magnitude is not high because of the elevated temperature, which assists in the smooth grain rotations. Moreover, the stress distribution (σ_{xx}) shows an overall compression (negative stress value) of the surface with small regions having positive stresses (refer Fig. 15(b)). This has caused slight distortions of the grains in the specimen with the formation of twin boundaries as shown in the orientation snapshot in Fig. 15(b). With increase in the reduction percent under larger strain, there is a sharp decrease in the atomic fraction with low angle rotations along with increase in the atomic fraction having 45°-degree rotation and few higher degree rotations as shown in the plot of Fig. 15(c). This finding indicates that the grain rotation has occurred along a single direction resulting in anisotropic orientation distribution. The stress distribution also shows a shift from the negative distribution towards a positive stress distribution in the specimen signifying that specimen has undergone stress relaxation after traversing out of the rollers. Moreover, it is found that rolling through the second set of rollers (high strain deformation) has also caused grain refinement at the surface and is shown in the orientation snapshot in Fig. 15(c). Similar type of deformation behavior and texture evolution is already observed during the experimental studies of rolling process and has been reported in literature [67].

3.4. Characterization of the rolled specimens through virtual diffraction analysis

Fig. 16 shows the XRD plots for the unrolled and rolled (first and second set of rollers) NC Ni specimens at different operating temperatures. It is observed that the initial diffraction patterns show small peaks for (111) and (311) planes along with a larger peak for the (200) plane. Upon rolling through the first set of rollers, the peak intensities of (111) and (200) planes is found to be increased at all the temperatures. Specifically, the amplitude of the (200) peak increases with the increase in the rolling temperature as shown in Fig. 16. The growing intensity of these diffraction with increase in temperature signifies that the preferred orientation of the grains become (200) upon rolling through the first set of rollers. Similar type of diffraction patterns has been observed during the experimental evaluation of crystalline materials at increasing temperatures [68]. With increase in the thickness reduction percent through second set of rollers, it is observed that the peak intensity of the (200) planes decreases drastically. At the same time, the diffraction peak intensity of the (111) plane further increases indicating that this plane becomes the preferred orientation. However, as the rolling temperature is increased, the amplitude diminishes and a splitting peak is formed at 900 K as shown in Fig. 16(c). It can be attributed to the high compressive deformation employed on the specimen that results in the change in the interlaminar spacing (or change in the orientation).

4. Conclusions

We have employed molecular dynamics (MD) simulations to model and analyze the nanoscale rolling deformation behavior in NC Ni specimen and study the effect of temperature on the structural evolution and overall grain orientation. Based on the obtained results through the various analysis that we have performed, the following conclusions can be drawn:

- At low temperatures, atomic stress distribution snapshots show localized residual compressive stress accumulation at the grain boundary and tensile residual stress at triple junctions after the specimen traverses through the first set of rollers. With increase in the thickness reduction, large dislocations are generated to accommodate the plastic strain leading to formation of tensile-compressive

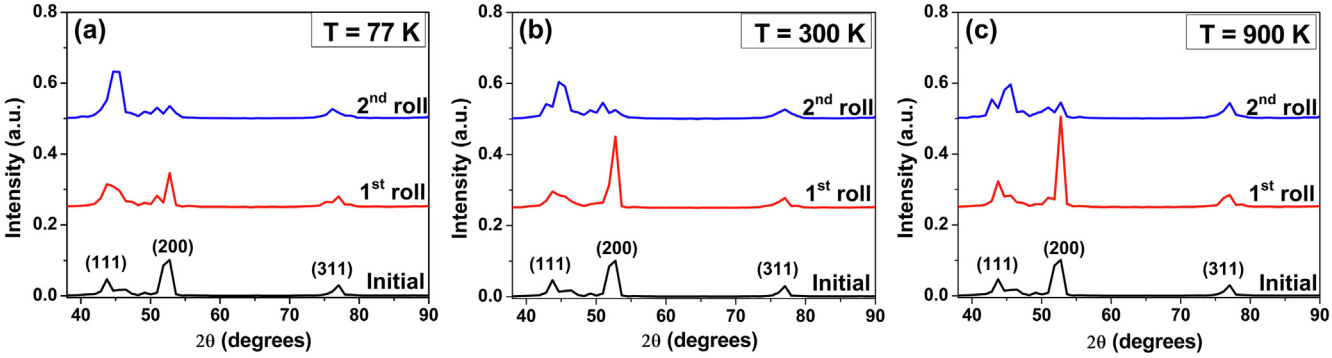

Fig. 16. XRD plots for the unrolled specimen, specimen rolled through first set of rollers, and specimen rolled through the second set of rollers at (a) 77 K, (b) 300 K, and (c) 900 K temperatures.

stress field.

- Atomic rotation analysis shows that low temperature rolling through first set of rollers have minimal change in the rotation angle with small orientation change. However, rolling through the second set of rollers show formation of new grain orientations along with the generation of finer grains, which are separated through sub-grain boundaries.
- At elevated temperatures, the interior of the specimen shows generation of the smaller and dispersed stresses attributed to the thermal vibrations caused by the high temperature deformation. However, at larger reduction percent, a tensile residual stress is generated after rolling because of the larger grain rotations and distortions, which is contrary to the low temperature deformation process.
- It has been found through atomic rotation analysis that magnitude of change in the rotation angle is higher at similar compressive stress due to high temperature. The atomic fraction with low angle rotation decreases and atomic fraction having 45° degree rotation increases indicating anisotropic orientation distribution. Moreover, orientation analysis has shown that the high compressive deformation has caused the grain refinement at the surface of the specimen after the rolling process.
- Virtual diffraction analysis shows an enhanced intensity of the (200) peak during the rolling through the first set of rollers indicating that the preferred orientation change. During the rolling through the second set of rollers, preferred orientations changes to (111) planes. The change in orientation is attributed to large compressive stress applied, which causes in the alteration of the interlaminar spacing and consequently change in the grain orientation.

CRediT authorship contribution statement

K. Vijay Reddy: Data curation, Formal analysis, Investigation, Methodology, Visualization, Writing - original draft. **Snehanshu Pal:** Conceptualization, Data curation, Funding acquisition, Investigation, Methodology, Project administration, Resources, Software, Supervision, Validation, Writing - review & editing.

Declaration of Competing Interest

The authors declare that they have no known competing financial interests or personal relationships that could have appeared to influence the work reported in this paper.

Acknowledgements

The authors like to recognize the aid provided by the Computer Centre of National Institute of Technology Rourkela by allowing the usage of high-performance computing facility (HPCF), which was necessary for carrying out the present research work.

Data availability

The raw/processed data required to reproduce these findings cannot be shared at this time as the data also forms part of an ongoing study.

Appendix A. Supplementary data

Supplementary data to this article can be found online at https://doi.org/10.1016/j.commatsci.2020.109935.

References

[1] U. Klement, U. Erb, A.M. El-Sherik, K.T. Aust, Thermal stability of nanocrystalline Ni, Mater. Sci. Eng. A 203 (1–2) (1995) 177–186.
[2] Y.M. Wang, A.V. Hamza, E. Ma, Temperature-dependent strain rate sensitivity and activation volume of nanocrystalline Ni, Acta Mater. 54 (10) (2006) 2715–2726.
[3] Y.M. Wang, E. Ma, On the origin of ultrahigh cryogenic strength of nanocrystalline metals, Appl. Phys. Lett. 85 (14) (2004) 2750–2752.
[4] S. Pal, K. Gururaj, M. Meraj, R.G. Bharadwaj, Molecular dynamics simulation study of uniaxial ratcheting behaviors for ultrafine-grained nanocrystalline nickel, J. Mater. Eng. Perform. 28 (8) (2019) 4918–4930.
[5] K.V. Reddy, S. Pal, Influence of dislocations, twins, and stacking faults on the fracture behavior of nanocrystalline Ni nanowire under constant bending load: a molecular dynamics study, J. Mol. Model. 24 (10) (2018) 277.
[6] K.V. Reddy, M. Meraj, S. Pal, Mechanistic study of bending creep behaviour of bi-crystal nanobeam, Comput. Mater. Sci. 136 (2017) 36–43.
[7] J.A. Lee, D.H. Lee, M.Y. Seok, I.C. Choi, H.N. Han, T.Y. Tsui, U. Ramamurty, J.I. Jang, Significant strengthening of nanocrystalline Ni sub-micron pillar by cyclic loading in elastic regime, Scr. Mater. 140 (2017) 31–34.
[8] U. Erb, Electrodeposited nanocrystals: synthesis, properties and industrial applications, Nanostruct. Mater. 6 (5–8) (1995) 533–538.
[9] L. Wang, J. Zhang, Z. Zeng, Y. Lin, L. Hu, Q. Xue, Fabrication of a nanocrystalline Ni–Co/CoO functionally graded layer with excellent electrochemical corrosion and tribological performance, Nanotechnology 17 (18) (2006) 4614.
[10] G. Palumbo, F. Gonzalez, A.M. Brennenstuhl, U. Erb, W. Shmayda, P.C. Lichtenberger, In-situ nuclear steam generator repair using electrodeposited nanocrystalline nickel, Nanostruct. Mater. 9 (1–8) (1997) 737–746.
[11] L. Zhu, O. Younes, N. Ashkenasy, Y. Shacham-Diamand, E. Gileadi, STM/AFM studies of the evolution of morphology of electroplated Ni/W alloys, Appl. Surf. Sci. 200 (1–4) (2002) 1–14.
[12] S. Zhang, S. Kobayashi, Multilayering process of electrodeposited nanocrystalline iron–nickel alloys for further strengthening, J. Mater. Sci. 55 (13) (2020) 5627–5638.
[13] T. K. Do, A. Lund, A reliability study of a new nanocrystalline nickel alloy barrier layer for electrical contacts, in: 2010 Proceedings of the 56th IEEE Holm Conference on Electrical Contacts, (2010) pp. 1-9.
[14] G. Zhang, W. Li, K. Xie, F. Yu, H. Huang, A one-step and binder-free method to fabricate hierarchical nickel-based supercapacitor electrodes with excellent performance, Adv. Funct. Mater. 23 (29) (2013) 3675–3681.
[15] A.M. El-Sherik, U. Erb, Synthesis of bulk nanocrystalline nickel by pulsed electrodeposition, J. Mater. Sci. 30 (22) (1995) 5743–5749.
[16] H. Li, F. Ebrahimi, Synthesis and characterization of electrodeposited nanocrystalline nickel–iron alloys, Mater. Sci. Eng. A 347 (1–2) (2003) 93–101.
[17] R. Mitra, R.A. Hoffman, A. Madan, J.R. Weertman, Effect of process variables on the structure, residual stress, and hardness of sputtered nanocrystalline nickel films, J. Mater. Res. 16 (4) (2001) 1010–1027.
[18] R. Valiev, Nanostructuring of metals by severe plastic deformation for advanced

properties, Nat. Mater. 3 (8) (2004) 511–516.
[19] Z. Liao, M. Polyakov, O.G. Diaz, D. Axinte, G. Mohanty, X. Maeder, J. Michler, M. Hardy, Grain refinement mechanism of nickel-based superalloy by severe plastic deformation-Mechanical machining case, Acta Mater. 180 (2019) 2–14.
[20] F. Ebrahimi, H.Q. Li, Structure and properties of electrodeposited nanocrystalline FCC Ni-Fe alloys, Rev. Adv. Mater. Sci. 5 (2) (2003) 134–138.
[21] F. Czerwinski, J.A. Szpunar, U. Erb, Structural and magnetic characterization of nanocrystalline Ni-20% Fe permalloy films, J. Mater. Sci.: Mater. Electron. 11 (3) (2000) 243–251.
[22] L. Jinlong, W. Zhuqing, L. Tongxiang, K. Suzuki, M. Hideo, Effect of tungsten on microstructures of annealed electrodeposited Ni-W alloy and its corrosion resistance, Surf. Coat. Technol. 337 (2018) 516–524.
[23] R.J. McCabe, I.J. Beyerlein, J.S. Carpenter, N.A. Mara, The critical role of grain orientation and applied stress in nanoscale twinning, Nat. Commun. 5 (1) (2014) 1–7.
[24] P.T. Probst, S. Sekar, T.A. König, P. Formanek, G. Decher, A. Fery, M. Pauly, Highly oriented nanowire thin films with anisotropic optical properties driven by the simultaneous influence of surface templating and shear forces, ACS Appl. Mater. Interfaces 10 (3) (2018) 3046–3057.
[25] S. Suwas, N.P. Gurao, Crystallographic texture of materials, J. Indian Inst. Sci. 88 (2) (2008) 151.
[26] F. Xu, F. Fang, Y. Zhu, X. Zhang, Study on crystallographic orientation effect on surface generation of aluminum in nano-cutting, Nanoscale Res. Lett. 12 (1) (2017) 289.
[27] T.H. Fang, W.J. Chang, Effects of AFM-based nanomachining process on aluminum surface, J. Phys. Chem. Solids 64 (6) (2003) 913–918.
[28] Z. Guo, Y. Tian, X. Liu, F. Wang, C. Zhou, D. Zhang, Experimental investigation of the tip based micro/nano machining, Appl. Surf. Sci. 426 (2017) 406–417.
[29] M. Sato, N. Tsuji, Y. Minaminob, Y. Koizumi, Formation of nanocrystalline surface layers in various metallic materials by near surface severe plastic deformation, Sci. Technol. Adv. Mater. 5 (1–2) (2004) 145–152.
[30] M. Yoshino, N. Umehara, S. Aravindan, Development of functional surface by nanoplastic forming, Wear 266 (5–6) (2009) 581–584.
[31] Y. Ye, S.Z. Kure-Chu, Z. Sun, X. Li, H. Wang, G. Tang, Nanocrystallization and enhanced surface mechanical properties of commercial pure titanium by electropulsing-assisted ultrasonic surface rolling, Mater. Des. 149 (2018) 214–227.
[32] L. Jinlong, L. Hongyun, The effects of cold rolling temperature on corrosion resistance of pure iron, Appl. Surf. Sci. 317 (2014) 125–130.
[33] D.J. Savage, I.J. Beyerlein, N.A. Mara, S.C. Vogel, R.J. McCabe, M. Knezevic, Microstructure and texture evolution in Mg/Nb layered materials made by accumulative roll bonding, Int. J. Plast. 125 (2020) 1–26.
[34] S. Takajo, C.N. Tomé, S.C. Vogel, I.J. Beyerlein, Texture simulation of a severely cold rolled low carbon steel using polycrystal modeling, Int. J. Plast. 109 (2018) 137–152.
[35] K.V. Reddy, S. Pal, Dynamic formation and destruction process of stacking fault tetrahedra in single-crystal Ni during nanoscale cryo-rolling, Philos. Mag. Lett. 99 (7) (2019) 253–260.
[36] K.V. Reddy, S. Pal, Nano-rolling: roller speed-dependent morphological evolution and mechanical properties enhancement in nanoscale Mg, JOM 71 (10) (2019) 3407–3416.
[37] K.V. Reddy, S. Pal, Dynamic probing of structural evolution of single crystal Fe during rolling process using atomistic simulation, Steel Res. Int. 90 (7) (2019) 1800636.
[38] K.V. Reddy, S. Pal, Structural evolution and dislocation behaviour during nano-rolling process of FCC metals: a molecular dynamics simulation based investigation, J. Appl. Phys. 125 (9) (2019) 095101.
[39] K.V. Reddy, S. Pal, Accumulative roll bonding of Cu–Zr nanolaminate: atomistic-scale investigation of structural evolution and grain orientation scatter dependence on rolling parameters, J. Appl. Phys. 127 (15) (2020) 154305.
[40] B. Deng, P.C. Hsu, G. Chen, B.N. Chandrashekar, L. Liao, Z. Ayitimuda, J. Wu, Y. Guo, L. Lin, Y. Zhou, M. Aisijiang, Q. Xie, Y. Cui, Z. Liu, H. Peng, Roll-to-roll encapsulation of metal nanowires between graphene and plastic substrate for high-performance flexible transparent electrodes, Nano Lett. 15 (6) (2015) 4206–4213.
[41] D. Goswami, J.C. Munera, A. Pal, B. Sadri, C.L.P. Scarpetti, R.V. Martinez, Roll-to-roll nanoforming of metals using laser-induced superplasticity, Nano Lett. 18 (6) (2018) 3616–3622.
[42] L. Chang, C.Y. Zhou, L.L. Wen, J. Li, X.H. He, Molecular dynamics study of strain rate effects on tensile behavior of single crystal titanium nanowire, Comput. Mater. Sci. 128 (2017) 348–358.
[43] K.V. Reddy, S. Pal, Influence of grain boundary complexion on deformation mechanism of high temperature bending creep process of Cu bicrystal, Trans. Indian Inst. Met. 71 (7) (2018) 1721–1734.
[44] K.V. Reddy, S. Pal, Shock velocity-dependent elastic-plastic collapse of pre-existing stacking fault tetrahedron in single crystal Cu, Comput. Mater. Sci. 172 (2020) 109390.
[45] V. Menon, S. James, Molecular dynamics simulation study of liquid-assisted laser beam micromachining process, J. Manuf. Mater. Process. 2 (3) (2018) 51.
[46] P.M. Larsen, S. Schmidt, J. Schiøtz, Robust structural identification via polyhedral template matching, Modell. Simul. Mater. Sci. Eng. 24 (5) (2016) 055007.
[47] R. Krakow, R.J. Bennett, D.N. Johnstone, Z. Vukmanovic, W. Solano-Alvarez, S.J. Lainé, J.F. Einsle, P.A. Midgley, C.M.F. Rae, R. Hielscher, On three-dimensional misorientation spaces, Proc. R. Soc. A 473 (2206) (2017) 20170274.
[48] A. Stukowski, V.V. Bulatov, A. Arsenlis, Automated identification and indexing of dislocations in crystal interfaces, Modell. Simul. Mater. Sci. Eng. 20 (8) (2012) 085007.
[49] Z.H. Hong, S.F. Hwang, T.H. Fang, Atomic-level stress calculation and surface roughness of film deposition process using molecular dynamics simulation, Comput. Mater. Sci. 48 (3) (2010) 520–528.
[50] S.P. Coleman, D.E. Spearot, L. Capolungo, Virtual diffraction analysis of Ni [0 1 0] symmetric tilt grain boundaries, Modell. Simul. Mater. Sci. Eng. 21 (5) (2013) 055020.
[51] S.P. Coleman, D.E. Spearot, Atomistic simulation and virtual diffraction characterization of homophase and heterophase alumina interfaces, Acta Mater. 82 (2015) 403–413.
[52] S. Plimpton, Fast parallel algorithms for short-range molecular dynamics, J. Comput. Phys. 117 (1) (1995) 1–19.
[53] S.R. Wilson, M.I. Mendelev, Anisotropy of the solid–liquid interface properties of the Ni–Zr B33 phase from molecular dynamics simulation, Philos. Mag. 95 (2) (2015) 224–241.
[54] P. Hirel, Atomsk: a tool for manipulating and converting atomic data files, Comput. Phys. Commun. 197 (2015) 212–219.
[55] S. Bargmann, B. Klusemann, J. Markmann, J.E. Schnabel, K. Schneider, C. Soyarslan, J. Wilmers, Generation of 3D representative volume elements for heterogeneous materials: a review, Prog. Mater. Sci. 96 (2018) 322–384.
[56] A. Stukowski, Visualization and analysis of atomistic simulation data with OVITO–the Open Visualization Tool, Modell. Simul. Mater. Sci. Eng. 18 (1) (2009) 015012.
[57] D.J. Evans, B.L. Holian, The nose–hoover thermostat, J. Chem. Phys. 83 (8) (1985) 4069–4074.
[58] J.D. Honeycutt, H.C. Andersen, Molecular dynamics study of melting and freezing of small Lennard-Jones clusters, J. Phys. Chem. 91 (19) (1987) 4950–4963.
[59] D. Liu, D. Liu, X. Zhang, C. Liu, N. Ao, Surface nanocrystallization of 17–4 precipitation-hardening stainless steel subjected to ultrasonic surface rolling process, Mater. Sci. Eng. A 726 (2018) 69–81.
[60] S. Thorat, M. Sadaiah, The effect of residual stresses, grain size, grain orientation, and hardness on the surface quality of Co–Cr L605 alloy in Photochemical Machining, J. Alloys Compd. 804 (2019) 84–92.
[61] I.A. Ovid'ko, A.G. Sheinerman, Nanoscale rotational deformation in solids at high stresses, Appl. Phys. Lett. 98(18) (2011) 181909.
[62] I.A. Ovid'Ko, A.G. Sheinerman, Nanoscale rotational deformation near crack tips in nanocrystalline solids, J. Phys. D: Appl. Phys. 45 (33) (2012) 335301.
[63] S.V. Bobylev, I.A. Ovid'Ko, Grain boundary rotations in solids, Phys. Rev. Lett. 109(17) (2012) 175501.
[64] X. Song, F. Wang, D. Qian, L. Hua, Tailoring the residual stress and mechanical properties by electroshocking treatment in cold rolled M50 steel, Mater. Sci. Eng. A 780 (2020) 139171.
[65] W. Yin, W. Wang, X. Fang, C. Qin, Annealing behavior at triple junctions in high-purity aluminum after slight cold rolling, J. Mater. Eng. Perform. 26 (4) (2017) 1506–1512.
[66] S. Miyazaki, K. Shibata, H. Fujita, Effect of specimen thickness on mechanical properties of polycrystalline aggregates with various grain sizes, Acta Metall. 27 (5) (1979) 855–862.
[67] J.A. Del Valle, M.T. Pérez-Prado, O.A. Ruano, Texture evolution during large-strain hot rolling of the Mg AZ61 alloy, Mater. Sci. Eng. A 355 (1–2) (2003) 68–78.
[68] D. Tahir, K. H. Jae, Effect of growth temperature on structural and electronic properties of ZnO thin films, in: AIP Conference Proceedings, 1801(1) (2017) pp. 020007.